This is the authors' version, post-peer reviewed, of the following article:
Nano Lett., 2018, 18 (3), pp 1751–1757
DOI: 10.1021/acs.nanolett.7b04868
Which has been published in final form at:
https://pubs.acs.org/doi/abs/10.1021/acs.nanolett.7b04868

Strain control of exciton-phonon coupling in atomically thin semiconductors

*Iris Niehues[1], Robert Schmidt[1], Matthias Drüppel[2], Philipp Marauhn[2], Dominik Christiansen[3], Malte Selig[3], Gunnar Berghäuser[3], Daniel Wigger[2], Robert Schneider[1], Lisa Braasch[1], Rouven Koch[1], Andres Castellanos-Gomez[4], Tilmann Kuhn[2], Andreas Knorr[3], Ermin Malic[5], Michael Rohlfing[2], Steffen Michaelis de Vasconcellos[1], and Rudolf Bratschitsch[1]**

[1]Institute of Physics and Center for Nanotechnology, University of Münster, D-48149 Münster, Germany

[2]Institute of Solid State Theory, University of Münster, D-48149 Münster, Germany

[3]Institut für Theoretische Physik, Nichtlineare Optik und Quantenelektronik, Technische Universität Berlin, D-10623 Berlin, Germany

[4]Materials Science Factory, Instituto de Ciencia de los Materiales de Madrid (ICMM-CSIC), Madrid, E-28049, Spain.

[5]Chalmers University of Technology, Department of Physics, SE-412 96 Gothenburg, Sweden

*e-mail: Rudolf.Bratschitsch@uni-muenster.de

Keywords: transition metal dichalcogenide, strain, excitons, line width, exciton-phonon coupling

This is the authors' version, post-peer reviewed, of the following article:
Nano Lett., 2018, 18 (3), pp 1751–1757
DOI: 10.1021/acs.nanolett.7b04868
Which has been published in final form at:
https://pubs.acs.org/doi/abs/10.1021/acs.nanolett.7b04868

Abstract

Semiconducting transition metal dichalcogenide (TMDC) monolayers have exceptional physical properties. They show bright photoluminescence due to their unique band structure and absorb more than 10% of the light at their excitonic resonances despite their atomic thickness. At room temperature, the width of the exciton transitions is governed by the exciton-phonon interaction leading to strongly asymmetric line shapes. TMDC monolayers are also extremely flexible, sustaining mechanical strain of about 10 % without breaking. The excitonic properties strongly depend on strain. For example, exciton energies of TMDC monolayers significantly redshift under uniaxial tensile strain. Here, we demonstrate that the width and the asymmetric line shape of excitonic resonances in TMDC monolayers can be controlled with applied strain. We measure photoluminescence and absorption spectra of the A exciton in monolayer $MoSe_2$, WSe_2, WS_2, and MoS_2 under uniaxial tensile strain. We find that the A exciton substantially narrows and becomes more symmetric for the selenium-based monolayer materials, while no change is observed for atomically thin WS_2. For MoS_2 monolayers, the line width increases. These effects are due to a modified exciton-phonon coupling at increasing strain levels because of changes in the electronic band structure of the respective monolayer materials. This interpretation based on steady-state experiments is corroborated by time-resolved photoluminescence measurements. Our results demonstrate that moderate strain values on the order of only 1% are already sufficient to globally tune the exciton-phonon interaction in TMDC monolayers and hold the promise for controlling the coupling on the nanoscale.

This is the authors' version, post-peer reviewed, of the following article:
Nano Lett., 2018, 18 (3), pp 1751–1757
DOI: 10.1021/acs.nanolett.7b04868
Which has been published in final form at:
https://pubs.acs.org/doi/abs/10.1021/acs.nanolett.7b04868

Uniaxial mechanical strain alters the lattice constants and reduces the symmetry in single crystals, leading to significant changes in the electronic band structure. The controlled application of strain to a material is therefore a powerful tool for tailoring its electronic and optical properties. For example, strain significantly increases the charge carrier mobility in the traditional semiconductors silicon and germanium[1]. Strained germanium nanomembranes even exhibit an indirect to direct band gap transistion[2]. Mechanical strain is also well-known to change the electronic phases of complex oxides. In that way, their fundamental bulk electronic properties such as superconductivity or magnetism can be strongly influenced[3–5]. Strain values on the order of a few percent are readily achievable by growing the oxides on lattice-mismatched substrates[6]. In contrast, two-dimensional materials, such as graphene or transition metal dichalcogenides (TMDCs), hold the promise for tunable strain control due to their atomic thickness and large flexibility[7,8]. In particular, the optical properties of these materials can be strongly modified[9,10]. For example, the fundamental resonances in TMDCs, called excitons, strongly downshift in energy with the application of uniaxial tensile strain[11–21]. Strain engineering might open the door to tune also the widths of the excitonic resonances which are exceedingly difficult to control by other means. At cryogenic temperatures, they were successfully narrowed down by reducing inhomogeneous broadening with encapsulation techniques[22–24]. At room temperature, however, the line width of the excitons in TMDCs is dominated by the electron-phonon interaction[25,26], which poses a fundamental lower limit on the line width. Here, we demonstrate that the electron-phonon interaction in 2D TMDCs can be engineered by mechanical strain. We find that the excitonic line width in WSe_2 and $MoSe_2$ monolayers can be substantially reduced by applying uniaxial tensile strain. In contrast, the line width stays constant for monolayer WS_2 and increases

This is the authors' version, post-peer reviewed, of the following article:
Nano Lett., 2018, 18 (3), pp 1751–1757
DOI: 10.1021/acs.nanolett.7b04868
Which has been published in final form at:
https://pubs.acs.org/doi/abs/10.1021/acs.nanolett.7b04868

for MoS_2. The main reason for these observed trends is the exciton-phonon coupling due to the change of the band structure under mechanical strain.

TMDC monolayers are micromechanically exfoliated[27] onto polydimethyldisiloxane (PDMS) and identified by reflection and photoluminescence (PL) microscopy. Subsequently, the atomically thin crystals are stamped on a flexible polycarbonate (PC) substrate of 500 µm thickness[28] and covered with a 160 µm thick PDMS layer to avoid slippage of the TMDC monolayers during the straining experiments[29,30]. Reversible uniaxial tensile strain is applied to the monolayers in a controlled way by bending the substrate[9].

We perform photoluminescence and absorption measurements of four different TMDC monolayers ($MoSe_2$, WSe_2, WS_2, and MoS_2) at room temperature to investigate the effect of mechanical strain on the A exciton. As previously reported[9], uniaxial tensile strain leads to a linear redshift of the A exciton energy for all materials in the strain range of less than 1.5 % (see supporting information Fig. S1 and S2). To highlight the influence of strain on the excitonic line shape, we normalize all PL spectra and shift them to the maximum of the A exciton (Fig. 1a-d). Exemplary spectra are shown for minimum (purple), medium (pink), and maximum (orange) strain.

This is the authors' version, post-peer reviewed, of the following article:
Nano Lett., 2018, 18 (3), pp 1751–1757
DOI: 10.1021/acs.nanolett.7b04868
Which has been published in final form at:
https://pubs.acs.org/doi/abs/10.1021/acs.nanolett.7b04868

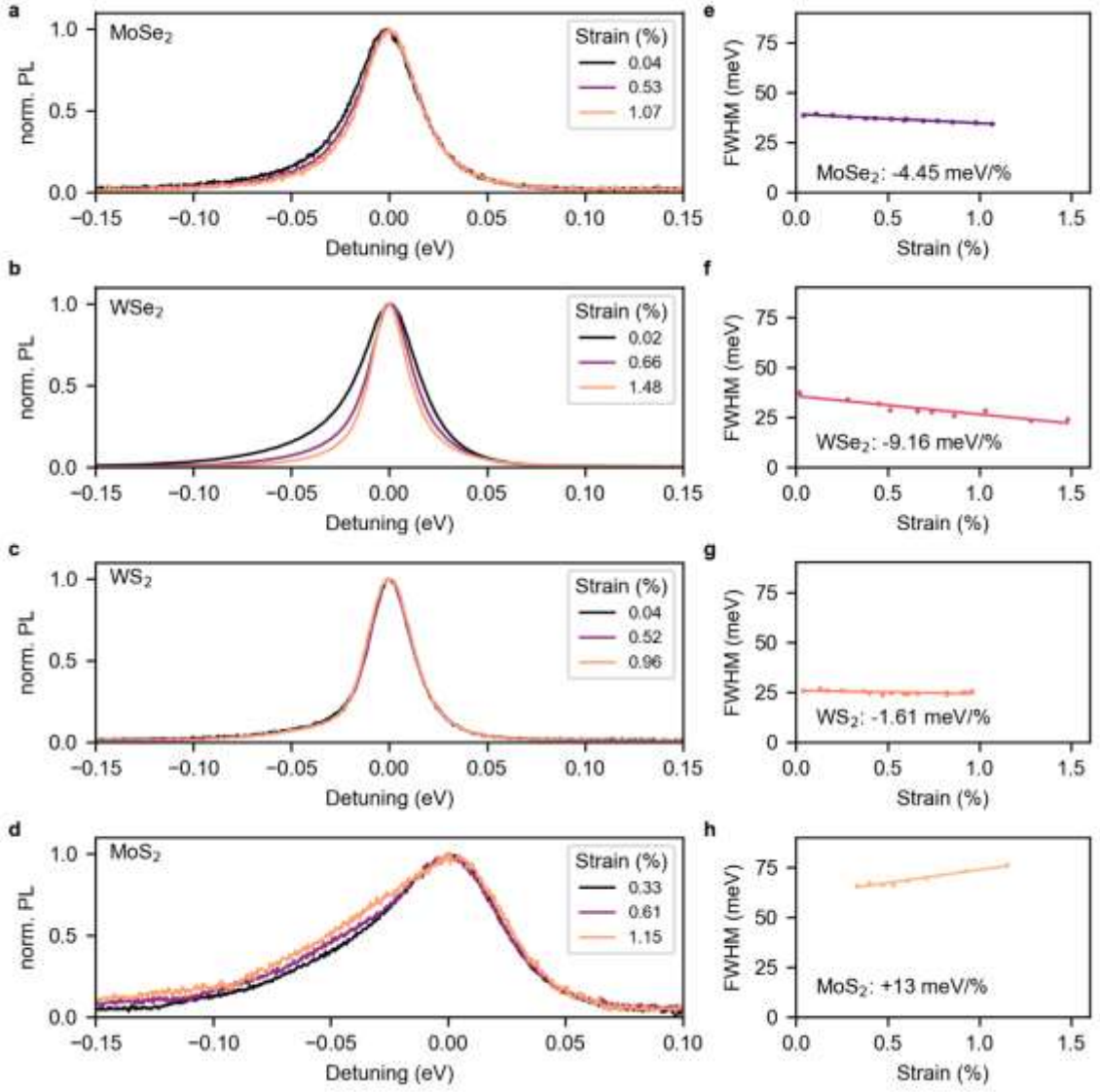

Figure 1: Photoluminescence (PL) spectra of TMDC monolayers under uniaxial tensile strain. **a**)-**d**) Normalized PL spectra of the A exciton for monolayer $MoSe_2$ (**a**), WSe_2 (**b**), WS_2 (**c**), and MoS_2 (**d**) for three exemplary strain levels. The spectra are horizontally shifted to pin the A exciton peak at the same position. **e-h**) Full width at half maximum (FWHM) line width of the spectra for increasing strain levels for the different materials. For $MoSe_2$ (**e**) and WSe_2 (**f**) the line width is decreasing with increasing strain ((-4.44±0.20) meV/% and (-9.16±1.35) meV/%, respectively) and the line shape becomes more symmetric, while for WS_2 (**g**) the line shape stays

This is the authors' version, post-peer reviewed, of the following article:
Nano Lett., 2018, 18 (3), pp 1751–1757
DOI: 10.1021/acs.nanolett.7b04868
Which has been published in final form at:
https://pubs.acs.org/doi/abs/10.1021/acs.nanolett.7b04868

almost constant (-1.61±0.86 meV/%). For MoS_2 (**h**), the line width increases with increasing strain (+13±1 meV/%).

In the unstrained case, the PL line shape is asymmetric for all four monolayer materials with a steeper slope on the high-energy side compared to the low-energy side. The line shape is dominated by asymmetric phonon sidebands due to the strong exciton-phonon coupling. The sidebands originate mainly from the emission and absorption of optical phonons[31]. For monolayer $MoSe_2$, the PL intensity of the low-energy side decreases with increasing tensile strain, while the high-energy side remains unchanged (Fig. 1a). For WSe_2 this effect is much more pronounced (Fig. 1b), and in addition, a narrowing on the high-energy side is observed. Consequently, the shape of the PL spectra for both materials becomes more symmetric with increasing strain. In strong contrast, no significant change of the line shape is observed for the WS_2 monolayer (Fig. 1c), and for MoS_2 the line shape even becomes more asymmetric due to a slightly increased PL intensity on the low-energy side (Fig. 1d).

To quantify the effect of strain on the exciton-phonon coupling in the TMDC monolayers, the full width at half maximum (FWHM) of the A exciton line is depicted in Fig. 1e-h for increasing uniaxial tensile strain levels. The value of the FWHM is determined by fitting the asymmetric line shape, which is described in detail in the supporting information in Fig. S3. For $MoSe_2$ (e) and WSe_2 (f) the line width decreases linearly with increasing strain in the examined range. The extracted gauge factors are (-4.44±0.20) meV/% and (-9.16±1.35) meV/% for monolayer $MoSe_2$ and WSe_2, respectively. For monolayer WS_2 (g), the line width remains almost unchanged at 25 meV (the gauge factor is -1.61±0.86 meV/%). In contrast, for monolayer MoS_2 (h), the line width increases with (+13±1) meV/%.

This is the authors' version, post-peer reviewed, of the following article:
Nano Lett., 2018, 18 (3), pp 1751–1757
DOI: 10.1021/acs.nanolett.7b04868
Which has been published in final form at:
https://pubs.acs.org/doi/abs/10.1021/acs.nanolett.7b04868

To verify the trends observed in emission, we also investigate the optical absorption using the same samples for all four atomically thin materials in Fig. 2. The optical absorption is derived from light transmitted through the TMDC monolayer T_{ml} normalized by the transmission through the substrate T_{sub}. The absorption spectrum is calculated via $A_{\mathrm{ml}} = 1 - \frac{T_{\mathrm{ml}}}{T_{\mathrm{sub}}}$, considering that the reflectivity of the monolayer is negligible compared to the absorption at the excitonic resonances[34]. Similar to the photoluminescence spectra, we find a prominent redshift of the A exciton resonance with gauge factors being in excellent agreement with the extracted values from the PL measurements and with calculations (see supporting information Fig. S2). In Fig. 2a-d the absorption spectra are presented for three different strain levels (minimum in purple, intermediate in pink, and maximum in orange) for the four materials. Again, the spectra are normalized and plotted against the detuning with respect to the A exciton maximum position to facilitate the comparison between spectra acquired at different strain levels highlight the effect of strain on the line shape.

This is the authors' version, post-peer reviewed, of the following article:
Nano Lett., 2018, 18 (3), pp 1751–1757
DOI: 10.1021/acs.nanolett.7b04868
Which has been published in final form at:
https://pubs.acs.org/doi/abs/10.1021/acs.nanolett.7b04868

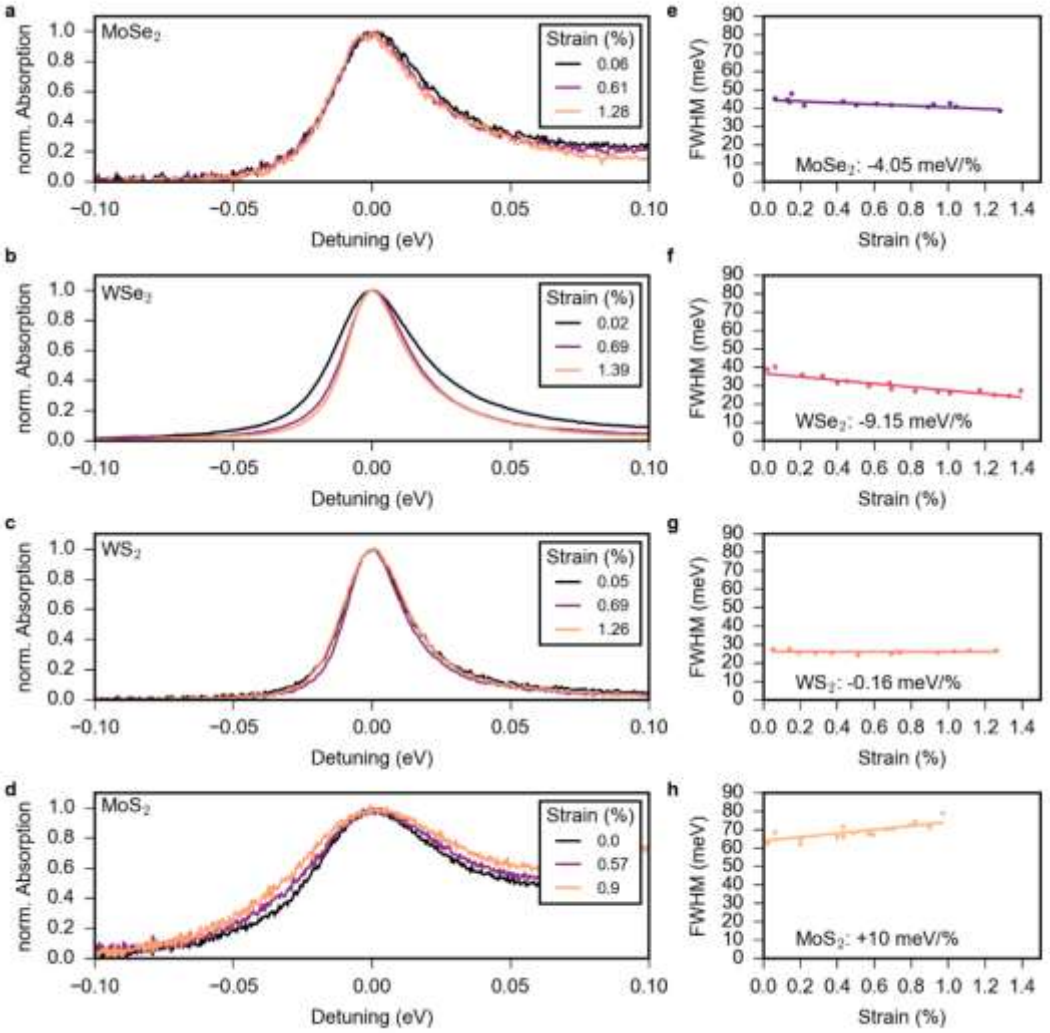

Figure 2: Absorption spectra of TMDC monolayers under uniaxial tensile strain. a)-d) Absorption spectra for monolayer $MoSe_2$ (**a**), WSe_2 (**b**), WS_2 (**c**), and MoS_2 (**d**) for 3 exemplary strain levels. The spectra are horizontally shifted to pin the A exciton peak at the same position. **e-h**) FWHM line width of the absorption spectra for increasing strain levels for the different materials. For $MoSe_2$ (**e**) and WSe_2 (**f**) the FWHM is decreasing with increasing strain ((-4.05±0.78) meV/% and (-9.25±1.44) meV/% respectively) and the spectral shape becomes more symmetric, while for WS_2 (**g**) no change is observed (-0.16±0.88 meV/%). Again, in MoS_2 (**h**) the line width is increasing (+10±2 meV/%) and the spectra become more asymmetric.

This is the authors' version, post-peer reviewed, of the following article:
Nano Lett., 2018, 18 (3), pp 1751–1757
DOI: 10.1021/acs.nanolett.7b04868
Which has been published in final form at:
https://pubs.acs.org/doi/abs/10.1021/acs.nanolett.7b04868

Contrary to light emission in Fig. 1, the high-energy side of the excitonic resonance is more pronounced in absorption. This is because the phonon creation processes appear at higher energies in absorption[35]. For the light emission spectra, this broadening appears on the low-energy side, because of its photon-emission character (see supporting information Fig. S4). In Fig. 2e-h the line width of the A exciton is plotted for all measured strain levels. As in the PL measurements, for $MoSe_2$ (e) and WSe_2 (f) a prominent decrease of the line width with increasing strain is observed with gauge factors of (-4.05±0.78) meV/% and (-9.25±1.44) meV/%, respectively. Again, for WS_2 (g) the line width is constant with (-0.16±0.88) meV/%, and for MoS_2 (h) an increase of (+10±2) meV/% is observed. The changes of the line shape of the A exciton with strain from emission (PL) and absorption measurements are in excellent quantitative agreement, which confirms the validity of our measurements. Only for monolayer MoS_2, the extracted change of the line width is stronger in the PL measurement compared to absorption (13 meV/% vs. 10 meV/%). We attribute this to the possible weak influence of the trion on the PL on monolayer MoS_2, which slightly broadens the spectra (see supporting information Fig. S5)[32]. However, a clear line broadening of the A exciton with uniaxial tensile strain is visible in both the PL and absorption measurement for monolayer MoS_2, while in the latter one the influence of the trion is negligible (see supporting information Fig. S4). In addition, all observed changes in the four investigated materials are reversible with strain (see supporting information Fig. S1 and S2).

We attribute the decrease or increase of the line widths of the A excitons under uniaxial tensile strain mainly to two different effects in the monolayers: changes in the electronic band structure and change of the phonon energies. They lead to a modification of the exciton-phonon coupling and alter the intravalley and intervalley scattering rates. Fig. 3 schematically depicts the different

This is the authors' version, post-peer reviewed, of the following article:
Nano Lett., 2018, 18 (3), pp 1751–1757
DOI: 10.1021/acs.nanolett.7b04868
Which has been published in final form at:
https://pubs.acs.org/doi/abs/10.1021/acs.nanolett.7b04868

exciton energy alignments and phonon scattering channels with and without strain for all four materials.

In monolayer $MoSe_2$ (Fig. 3a), intervalley scattering is very unlikely, because the indirect KΛ exciton has a much larger energy than the KK exciton. Additional strain shifts it to even higher values. Therefore, intravalley scattering of the excitons with phonons solely governs the excitonic line width at room temperature[31]. It leads to the pronounced asymmetry in the line shape at the high-energy side of the absorption spectrum (see supporting information Fig. S6a for details). The observation that the A exciton line shape of monolayer $MoSe_2$ becomes more symmetric and narrower with increasing strain can be explained by a decrease of the exciton-phonon coupling. By applying uniaxial strain to the monolayer, the longitudinal-optical phonon bands split into two branches, with one branch shifting towards higher and the other towards lower energies[36,37]. The calculated splitting of the phonon branches is on the order of 3 to 10 cm^{-1} at 2% of uniaxial strain[36], which has been confirmed by experiments[38]. The model described in Ref.[26] demonstrates that the coupling strength increases with lower phonon energies and decreases with higher phonon energies. Therefore, the strain-induced shift to lower/higher phonon energies renders exciton scattering with phonons more/less probable. At the same time, the phonon population increases/decreases, which increases/decreases the scattering probability[26,31]. Since our measurements show a line narrowing with increasing uniaxial tensile strain, we conclude that the influence of the energetically higher phonon branches, which decrease the scattering processes, dominates. For acoustic phonons, previous calculations predict no significant change in the dispersion at 1% of strain. Only at much higher strain values (>7%) the slope of the phonon branches shift to lower values[39,40]. Overall, our measurements indicate that intravalley scattering

This is the authors' version, post-peer reviewed, of the following article:
Nano Lett., 2018, 18 (3), pp 1751–1757
DOI: 10.1021/acs.nanolett.7b04868
Which has been published in final form at:
https://pubs.acs.org/doi/abs/10.1021/acs.nanolett.7b04868

becomes less probable in monolayer $MoSe_2$ with increasing strain and thus the reduction of the exciton linewidth is due to a decrease of the exciton-phonon coupling upon straining.

In contrast to $MoSe_2$, intervalley scattering processes play an important role for WSe_2 monolayers. Excitons are effectively scattered by phonons from the bright KK to the dark KΛ exciton state, because the KΛ state lies energetically below the KK exciton state at zero strain[31] as sketched in Fig. 3b. While intravalley scattering broadens the high-energy side of the A exciton (similar to $MoSe_2$), intervalley scattering processes lead to an additional broadening of the low-energy side of the spectra (Fig. S6b). As a consequence, both sides of the A exciton line are broadened at zero strain[26,31]. With increasing strain, our measurements indicate that for monolayer WSe_2 both the low- and high-energy side of the A exciton narrows (Fig. 1b), which demonstrates that strain also influences intervalley scattering. This narrowing can be tracked down to the change in the band structure of the WSe_2 monolayer under the influence of uniaxial tensile strain, where the KΛ state approaches the energy of the KK state (Fig. 3b and supporting information Fig. S7). Since both scattering processes (intravalley and intervalley) contribute about equally to the line width of monolayer WSe_2 at room temperature[26], the measured narrowing gauge factor of monolayer WSe_2 (-9 meV/%) becomes about twice as large as for $MoSe_2$ (-4 meV/%).

This is the authors' version, post-peer reviewed, of the following article:
Nano Lett., 2018, 18 (3), pp 1751–1757
DOI: 10.1021/acs.nanolett.7b04868
Which has been published in final form at:
https://pubs.acs.org/doi/abs/10.1021/acs.nanolett.7b04868

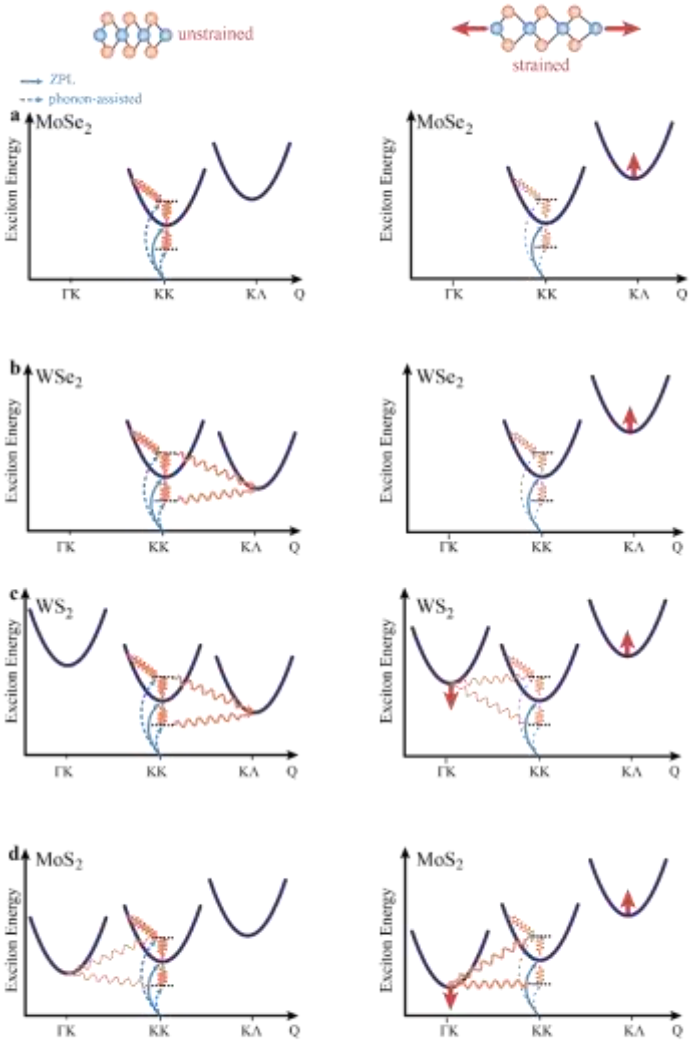

Figure 3: Schematic drawing of the exciton-phonon scattering mechanisms in monolayer TMDCs without and with applied uniaxial tensile strain. In the unstrained case (left column) intravalley scattering dominates the spectral shape of $MoSe_2$ (a) and MoS_2 (d), while for WSe_2 (b) and WS_2 (c) also intervalley scattering plays an important role, because the KΛ state lies energetically below the KK state. With applied strain (right column) the band structure and the exciton-phonon coupling changes in a different way for the four materials. For all materials, the intravalley scattering decreases. Furthermore, the KΛ state lies energetically higher than the KK state. Therefore, the intervalley scattering decreases in tungsten-based materials (b, c). For sulfur-

This is the authors' version, post-peer reviewed, of the following article:
Nano Lett., 2018, 18 (3), pp 1751–1757
DOI: 10.1021/acs.nanolett.7b04868
Which has been published in final form at:
https://pubs.acs.org/doi/abs/10.1021/acs.nanolett.7b04868

based materials (c, d) also the ΓK exciton plays a role, which is decreasing with strain and opens a new scattering channel.

In monolayer WSe_2 (and WS_2) the spin-forbidden dark exciton states lie energetically below the bright ones[41–43]. They have a negligible effect on the excitonic line shape of bright excitons, because the required spin-flip process occur on a much slower time scale compared to phonon-assisted processes[31,44]. Therefore, the overall narrowing trend of the A exciton with increasing strain can be witnessed in both $MoSe_2$ and WSe_2 monolayers, although both materials exhibit a different spin ordering in the conduction band.

In WS_2 (Fig. 3c) and MoS_2 (Fig. 3d) monolayers the situation for the KK and the KΛ exciton and their coupling to phonons is the same as for the selenium-based counterparts. But in sulfur-based materials a third exciton has to be taken into account, the one formed by the hole located in the Γ valley and the electron in the K valley. For WS_2 this dark transition lies energetically slightly above the bright KK exciton, and in MoS_2 slightly below[45]. This opens a new scattering channel for excitons in MoS_2 even at zero strain, which can explain the observed broad line width together with the high density of defects[46] leading to substantial inhomogeneous broadening in this material.

In monolayer WS_2 (Fig. 3c), surprisingly, no change of the exciton line width with increasing strain is measured. An important clue to understand this behavior is the much weaker exciton-phonon coupling compared to the other TMDCs. Sulfur-based TMDCs exhibit less efficient exciton-phonon scattering compared to selenium-based compounds because of the higher phonon energies[47]. Indeed, the exciton line width of monolayer WS_2 is already rather small at zero strain (25 meV), compared to monolayer $MoSe_2$ and WSe_2 (39 meV and 36 meV). Furthermore, the indirect ΓK exciton decreases in energy upon applied strain, because of an upshift of the valence

This is the authors' version, post-peer reviewed, of the following article:
Nano Lett., 2018, 18 (3), pp 1751–1757
DOI: 10.1021/acs.nanolett.7b04868
Which has been published in final form at:
https://pubs.acs.org/doi/abs/10.1021/acs.nanolett.7b04868

band at the Γ point, which may open a new scattering channel (see Supporting Information Fig. S7). Therefore, there are now two counteracting contributions of increased (ΓK exciton) and decreased (KΛ and KK exciton) phonon scattering. The almost unchanged line shape of monolayer WS_2 with increasing strain seems to be due to this peculiar situation where the two contributions are balanced.

Finally, the measured increase of the line width of the A exciton in monolayer MoS_2 can be understood by an upshift of the valence band at the Γ point. The ΓK exciton energy decreases and leads to enhanced exciton-phonon scattering into the ΓK state (Fig. 3d). Already at around 0.1% tensile strain, monolayer MoS_2 undergoes a direct to indirect transition[13]. The additional intervalley scattering increases under strain, and this broadening of the line width overcompensates the effect of the decrease in intravalley scattering in MoS_2.

To corroborate the change of the exciton-phonon coupling directly in the time domain, we perform time-resolved photoluminescence (TRPL) measurements for various strain levels (see the Supporting Information for experimental details) for $MoSe_2$, WSe_2, and WS_2 monolayers. For monolayer MoS_2, the dynamics is too fast to be resolved by the experimental setup. In Fig. 4a-c the PL dynamics are shown for three different strain values for $MoSe_2$, WSe_2, and WS_2, respectively.

This is the authors' version, post-peer reviewed, of the following article:
Nano Lett., 2018, 18 (3), pp 1751–1757
DOI: 10.1021/acs.nanolett.7b04868
Which has been published in final form at:
https://pubs.acs.org/doi/abs/10.1021/acs.nanolett.7b04868

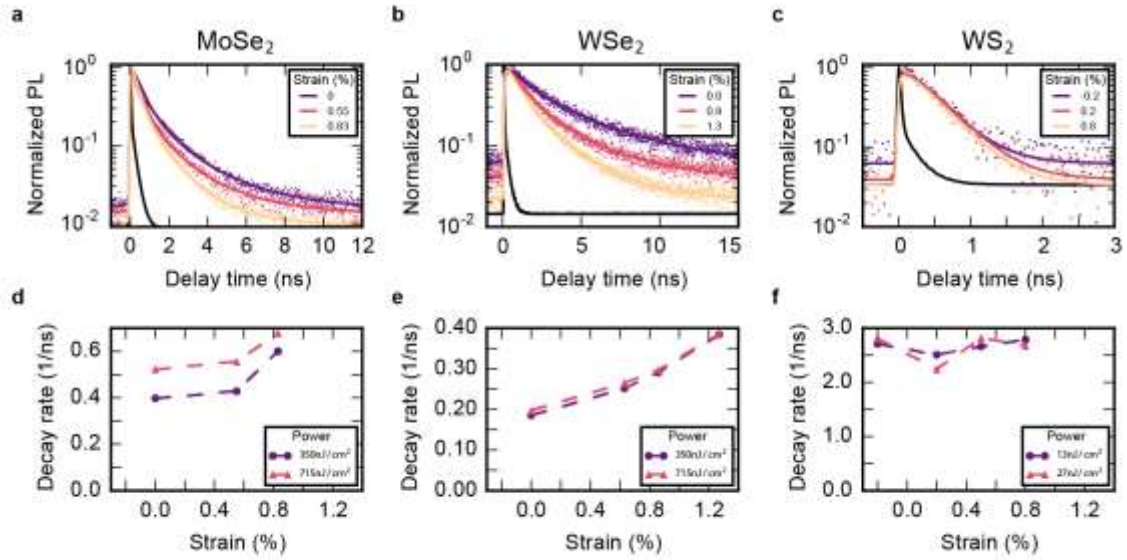

Figure 4: Time-resolved photoluminescence of TMDC monolayers under uniaxial tensile strain. a)-c) Time-resolved photoluminescence measurements for monolayer $MoSe_2$ (**a**), WSe_2 (**b**), and WS_2 (**c**) for 3 different strain levels (dots) with fits (solid lines). The instrument response function (IRF) is drawn in black. **d)-f)** PL decay rate extracted from **a)-c)** for increasing strain levels and low power (purple circles) and high power (orange triangles). For $MoSe_2$ (**c**) and WSe_2 (**d**) the decay rate is increasing with increasing strain ((0.21 +- 0.04) ns/% and (0.15+-0.01) ns/% respectively, while for WS_2 (**f**) no change is observed.

For both $MoSe_2$ (Fig. 4a) and WSe_2 (Fig. 4b), the decay of the PL signal of the A exciton becomes faster with increasing strain. To analyze the TRPL data in detail, the measured curves are fitted with a single exponential decay and including the exciton-exciton annihilation process. For each strain level, the PL decay is recorded for two laser powers to show the influence of the optically excited exciton density (see Supporting Information for more details). The corresponding extracted decay rates are displayed in Fig. 4c-d. For $MoSe_2$ (d) the PL decay rate increases with (0.21±0.01) ns^{-1}/% and for WSe_2 (e) with (0.15±0.01) ns^{-1}/% with increasing strain. In general, PL decay rates are strongly influenced by scattering of excitons out of the light cone, either by

This is the authors' version, post-peer reviewed, of the following article:
Nano Lett., 2018, 18 (3), pp 1751–1757
DOI: 10.1021/acs.nanolett.7b04868
Which has been published in final form at:
https://pubs.acs.org/doi/abs/10.1021/acs.nanolett.7b04868

intravalley scattering[48] or intervalley scattering[26,49]. Both the intra- and intervalley exciton-phonon scattering into dark states become less efficient with increasing strain. Therefore, more excitons remain within the light cone, which results in a faster PL decay. The increase of the decay rates for $MoSe_2$ and WSe_2 with increasing strain therefore nicely corresponds with the narrowing of their line widths. In the same way, the constant PL decay rate for monolayer WS_2 is in good agreement with the time-integrated PL measurements, where no change in the line width of WS_2 is observed with increasing strain. In WS_2 monolayers no significant change in the exciton-phonon coupling is observable for the considered strain levels. For monolayer MoS_2, the decay time of the A exciton is in the order of a few picoseconds at zero strain[50] and below the time resolution of our experimental setup. We would expect a decrease of the decay rate with increasing strain from our considerations above, deduced from our integrated PL measurements.

In summary, our results highlight the influence of mechanical strain of the exciton-phonon interaction in atomically thin TMDCs. We find that the A exciton line substantially narrows and becomes more symmetric for selenium-based TMDCs, because of the weakening of the exciton-phonon coupling with increasing strain. Indeed, at room temperature, a moderate amount of mechanical strain may be used to strongly narrow excitonic lines on the order of 10 meV/%. We envision that our newly found intrinsic line narrowing mechanism could be readily exploited without a strain apparatus, by growing the atomically thin TMDCs directly onto different substrates at high temperatures and inducing strain in the monolayers by the different thermal expansion coefficients of TMDC monolayer and substrate[51]. For WS_2 monolayers, no change in the excitonic line width and life time is observed due to the already weak exciton-phonon coupling in this material. In MoS_2, the line width increases, because of the change from a direct to an indirect semiconductor under tensile strain and the enhanced electron-phonon coupling. In contrast to these

This is the authors' version, post-peer reviewed, of the following article:
Nano Lett., 2018, 18 (3), pp 1751–1757
DOI: 10.1021/acs.nanolett.7b04868
Which has been published in final form at:
https://pubs.acs.org/doi/abs/10.1021/acs.nanolett.7b04868

global strain phenomena, it has been shown that local strain plays an important role for the formation of single-photon emitters in monolayer TMDCs[10,52–55]. Hence, our work also provides first clues towards understanding the influence of strain on the fundamental exciton-phonon coupling in these nanoscopic light emitters and thereby paves the way to tailoring local strain environments on the nanoscale.

ASSOCIATED CONTENT

Supporting Information.

- Photoluminescence under strain: A exciton resonance gauge factor
- Absorption under strain: A exciton resonance gauge factor
- Fitting of the PL and absorption spectra
- Asymmetry of PL and Absorption
- Valley positions under uniaxial strain
- Time resolved PL measurements (methods)
- Phonon contributions to the line width at zero strain

AUTHOR INFORMATION

Corresponding Author

Email: Rudolf.Bratschitsch@uni-muenster.de

ORCID

Rudolf Bratschitsch: 0000-0002-2368-2548

Andres Castellanos-Gomez: 0000-0002-3384-3405

Steffen Michaelis de Vasconcellos: 0000-0003-3584-0635

Iris Niehues: 0000-0001-7438-2679

Robert Schmidt: 0000-0002-8856-3347

Malte Selig: 0000-0003-0022-412X

Author Contributions

The manuscript was written with contributions of all authors. All authors have given approval to the final version of the manuscript.

Funding Sources

A.K, M.S and D.C acknowledge support by the Deutsche Forschungsgemeinschaft (DFG) through SFB 951 (A.K), SFB 910 (D.C) and SFB 787 (M.S). M.S gratefully acknowledges financial support of the School of Nanophotonics of the SFB 787. E.M and G.B were supported by funding from the European Union Horizon 2020 research and innovation program under grant agreement No 696656 (Graphene Flagship) and the Swedish Research Council (VR).

ABBREVIATIONS

PL photoluminescence, TRPL time resolved photoluminescence, TMDC transition metal dichalcogenide

REFERENCES

(1) Lee, M. L.; Fitzgerald, E. A.; Bulsara, M. T.; Currie, M. T.; Lochtefeld, A. *J. Appl. Phys.* **2005**, *97* (1), 1.

(2) Sanchez-Perez, J. R.; Boztug, C.; Chen, F.; Sudradjat, F. F.; Paskiewicz, D. M.; Jacobson,

R.; Lagally, M. G.; Paiella, R. *Proc. Natl. Acad. Sci.* **2011**, *108* (47), 18893–18898.

(3) Schuller, I. K. *Nature* **1998**, *394* (July), 4–5.

(4) Choi, K. J. *Science (80-.).* **2004**, *306* (5698), 1005–1009.

(5) Lee, J. H.; Fang, L.; Vlahos, E.; Ke, X.; Jung, Y. W.; Kourkoutis, L. F.; Kim, J.-W.; Ryan, P. J.; Heeg, T.; Roeckerath, M.; Goian, V.; Bernhagen, M.; Uecker, R.; Hammel, P. C.; Rabe, K. M.; Kamba, S.; Schubert, J.; Freeland, J. W.; Muller, D. A.; Fennie, C. J.; Schiffer, P.; Gopalan, V.; Johnston-Halperin, E.; Schlom, D. G. *Nature* **2011**, *476* (7358), 114–114.

(6) Burganov, B.; Adamo, C.; Mulder, A.; Uchida, M.; King, P. D. C.; Harter, J. W.; Shai, D. E.; Gibbs, A. S.; Mackenzie, A. P.; Uecker, R.; Bruetzam, M.; Beasley, M. R.; Fennie, C. J.; Schlom, D. G.; Shen, K. M. *Phys. Rev. Lett.* **2016**, *197003* (May), 1–6.

(7) Ghorbani-Asl, M.; Borini, S.; Kuc, A.; Heine, T. *Phys. Rev. B - Condens. Matter Mater. Phys.* **2013**, *87* (23), 1–6.

(8) Polyzos, I.; Bianchi, M.; Rizzi, L.; Koukaras, E. N.; Parthenios, J.; Papagelis, K.; Sordan, R.; Galiotis, C. *Nanoscale* **2015**, *7* (30), 13033–13042.

(9) Roldán, R.; Castellanos-Gomez, A.; Cappelluti, E.; Guinea, F. *J. Phys. Condens. Matter* **2015**, *27* (31), 313201.

(10) Kern, J.; Niehues, I.; Tonndorf, P.; Schmidt, R.; Wigger, D.; Schneider, R.; Stiehm, T.; Michaelis de Vasconcellos, S.; Reiter, D. E.; Kuhn, T.; Bratschitsch, R. *Adv. Mater.* **2016**, *28* (33), 7101–7105.

(11) He, K.; Poole, C.; Mak, K. F.; Shan, J. *Nano Lett.* **2013**, *13* (6), 2931–2936.

(12) Zhu, C. R.; Wang, G.; Liu, B. L.; Marie, X.; Qiao, X. F.; Zhang, X.; Wu, X. X.; Fan, H.; Tan, P. H.; Amand, T.; Urbaszek, B. *Phys. Rev. B* **2013**, *88* (12), 121301.

(13) Conley, H. J.; Wang, B.; Ziegler, J. I.; Haglund Jr, R. F.; Pantelides, S. T.; Bolotin, K. I.

Nano Lett. **2013**, *13* (8), 3626–3630.

(14) Castellanos-Gomez, A.; Roldán, R.; Cappelluti, E.; Buscema, M.; Guinea, F.; van der Zant, H. S. J.; Steele, G. A. *Nano Lett.* **2013**, *13* (11), 5361–5366.

(15) Desai, S. B.; Seol, G.; Kang, J. S.; Fang, H.; Battaglia, C.; Kapadia, R.; Ager, J. W.; Guo, J.; Javey, A. *Nano Lett.* **2014**, *14* (8), 4592–4597.

(16) Amin, B.; Kaloni, T. P.; Schwingenschlögl, U. *RSC Adv.* **2014**, *4* (65), 34561.

(17) Plechinger, G.; Castellanos-Gomez, A.; Buscema, M.; van der Zant, H. S. J.; Steele, G. A.; Kuc, A.; Heine, T.; Schüller, C.; Korn, T. *2D Mater.* **2015**, *2* (1), 15006.

(18) Wang, Y.; Cong, C.; Yang, W.; Shang, J.; Peimyoo, N.; Chen, Y.; Kang, J.; Wang, J.; Huang, W.; Yu, T. *Nano Res.* **2015**, *8* (8), 2562–2572.

(19) Island, J. O.; Kuc, A.; Diependaal, E. H.; Bratschitsch, R.; van der Zant, H. S. J.; Heine, T.; Castellanos-Gomez, A. *Nanoscale* **2016**, *8* (5), 2589–2593.

(20) Schmidt, R.; Niehues, I.; Schneider, R.; Drüppel, M.; Deilmann, T.; Rohlfing, M.; de Vasconcellos, S. M.; Castellanos-Gomez, A.; Bratschitsch, R. *2D Mater.* **2016**, *3* (2), 21011.

(21) Feierabend, M.; Morlet, A.; Berghäuser, G.; Malic, E. *Phys. Rev. B* **2017**, *96* (4), 1–7.

(22) Cadiz, F.; Courtade, E.; Robert, C.; Wang, G.; Shen, Y.; Cai, H.; Taniguchi, T.; Watanabe, K.; Carrere, H.; Lagarde, D.; Manca, M.; Amand, T.; Renucci, P.; Tongay, S.; Marie, X.; Urbaszek, B. *Phys. Rev. X* **2017**, *7* (2), 1–12.

(23) Ajayi, O. A.; Ardelean, J. V; Shepard, G. D.; Wang, J.; Antony, A.; Taniguchi, T.; Watanabe, K.; Heinz, T. F.; Strauf, S.; Zhu, X.-Y.; Hone, J. C. *2D Mater.* **2017**, *4* (3), 31011.

(24) Wierzbowski, J.; Klein, J.; Sigger, F.; Straubinger, C.; Kremser, M.; Taniguchi, T.; Watanabe, K.; Wurstbauer, U.; Holleitner, A. W.; Kaniber, M.; Müller, K.; Finley, J. J. **2017**.

(25) Christiansen D., Selig M., Berghäuser G., Schmidt R., Niehues I., Schneider R., Arora A., Michaelis de Vasconcellos M., Bratschitsch R., Malic E., K. A. *Phys. Rev. Lett.* **2017**, 1–6.

(26) Selig, M.; Berghäuser, G.; Raja, A.; Nagler, P.; Schüller, C.; Heinz, T. F.; Korn, T.; Chernikov, A.; Malic, E.; Knorr, A. *Nat. Commun.* **2016**, *7*.

(27) Tonndorf, P.; Schmidt, R.; Böttger, P.; Zhang, X.; Börner, J.; Liebig, A.; Albrecht, M.; Kloc, C.; Gordan, O.; Zahn, D. R. T.; others. *Opt. Express* **2013**, *21* (4), 4908–4916.

(28) Castellanos-Gomez, A.; Buscema, M.; Molenaar, R.; Singh, V.; Janssen, L.; van der Zant, H. S. J.; Steele, G. a. *2D Mater.* **2014**, *1* (1), 11002.

(29) Island, J. O.; Kuc, A.; Diependaal, E. H.; Bratschitsch, R.; van der Zant, H. S. J.; Heine, T.; Castellanos-Gomez, A. *Nanoscale* **2016**, *8* (5), 2589–2593.

(30) Schmidt, R.; Niehues, I.; Schneider, R.; Drüppel, M.; Deilmann, T.; Rohlfing, M.; de Vasconcellos, S. M.; Castellanos-Gomez, A.; Bratschitsch, R. *2D Mater.* **2016**, *3* (2), 21011.

(31) Christiansen, D.; Selig, M.; Berghäuser, G.; Schmidt, R.; Niehues, I.; Schneider, R.; Arora, A.; de Vasconcellos, S. M.; Bratschitsch, R.; Malic, E.; Knorr, A. *Phys. Rev. Lett.* **2017**, *119* (18), 187402.

(32) Mak, K. F.; He, K.; Lee, C.; Lee, G. H.; Hone, J.; Heinz, T. F.; Shan, J. *Nat. Mater.* **2012**, *12* (3), 207–211.

(33) Zhang, Y.; Li, H.; Wang, H.; Liu, R.; Zhang, S. L.; Qiu, Z. J. *ACS Nano* **2015**, *9* (8), 8514–8519.

(34) Li, Y.; Chernikov, A.; Zhang, X.; Rigosi, A.; Hill, H. M.; Van Der Zande, A. M.; Chenet, D. A.; Shih, E. M.; Hone, J.; Heinz, T. F. *Phys. Rev. B - Condens. Matter Mater. Phys.* **2014**, *90* (20), 1–6.

(35) Förstner, J.; Ahn, K. J.; Danckwerts, J.; Schaarschmidt, M.; Waldmüller, I.; Weber, C.;

Knorr, A. *Phys. Status Solidi Basic Res.* **2002**, *234* (1), 155–165.

(36) Chang, C. H.; Fan, X.; Lin, S. H.; Kuo, J. L. *Phys. Rev. B - Condens. Matter Mater. Phys.* **2013**, *88* (19), 1–9.

(37) Sahin, H.; Tongay, S.; Horzum, S.; Fan, W.; Zhou, J.; Li, J.; Wu, J.; Peeters, F. M. *Phys. Rev. B - Condens. Matter Mater. Phys.* **2013**, *87* (16), 1–6.

(38) Wang, Y. L.; Cong, C. X.; Qiu, C. Y.; Yu, T. *Small* **2013**, *9* (17), 2857–2861.

(39) Li, T. *Phys. Rev. B - Condens. Matter Mater. Phys.* **2012**, *85* (23), 1–5.

(40) Horzum, S.; Sahin, H.; Cahangirov, S.; Cudazzo, P.; Rubio, A.; Serin, T.; Peeters, F. M. *Phys. Rev. B - Condens. Matter Mater. Phys.* **2013**, *87* (12), 1–5.

(41) Zhang, X. X.; You, Y.; Zhao, S. Y. F.; Heinz, T. F. *Phys. Rev. Lett.* **2015**, *115* (25), 257403.

(42) Echeverry, J. P.; Urbaszek, B.; Amand, T.; Marie, X.; Gerber, I. C. *Phys. Rev. B* **2016**, *93* (12), 121107.

(43) Molas, M. R.; Faugeras, C.; Slobodeniuk, A. O.; Nogajewski, K.; Bartos, M.; Basko, D. M.; Potemski, M. *2D Mater.* **2017**, *4* (2), 21003.

(44) Glazov, M. M.; Amand, T.; Marie, X.; Lagarde, D.; Bouet, L.; Urbaszek, B. *Phys. Rev. B - Condens. Matter Mater. Phys.* **2014**, *89* (20), 1–5.

(45) Malic, E.; Selig, M.; Feierabend, M.; Brem, S.; Christiansen, D.; Wendler, F.; Knorr, A.; Berghäuser, G. **2017**, 1–7.

(46) Vancsó, P.; Magda, G. Z.; Pető, J.; Noh, J.-Y.; Kim, Y.-S.; Hwang, C.; Biró, L. P.; Tapasztó, L. *Sci. Rep.* **2016**, *6* (1), 29726.

(47) Jin, Z.; Li, X.; Mullen, J. T.; Kim, K. W. *Phys. Rev. B* **2014**, *90* (4), 45422.

(48) Poellmann, C.; Steinleitner, P.; Leierseder, U.; Nagler, P.; Plechinger, G.; Porer, M.; Bratschitsch, R.; Schüller, C.; Korn, T.; Huber, R. *Nat. Mater.* **2015**, *14* (July), 1–6.

(49) Selig, M.; Berghäuser, G.; Richter, M.; Bratschitsch, R.; Knorr, A.; Malic, E. **2017**, 1–8.

(50) Mak, K. F.; He, K.; Shan, J.; Heinz, T. F. *Nat. Nanotechnol.* **2012**, *7* (8), 494–498.

(51) Ahn, G. H.; Amani, M.; Rasool, H.; Lien, D.-H.; Mastandrea, J. P.; Ager III, J. W.; Dubey, M.; Chrzan, D. C.; Minor, A. M.; Javey, A. *Nat. Commun.* **2017**, *8* (1), 608.

(52) Tonndorf, P.; Schmidt, R.; Schneider, R.; Kern, J.; Buscema, M.; Steele, G. A.; Castellanos-Gomez, A.; van der Zant, H. S. J.; de Vasconcellos, S. M.; Bratschitsch, R. *Optica* **2015**, *2* (4), 347–352.

(53) Kumar, S.; Kaczmarczyk, A.; Gerardot, B. D. *Nano Lett.* **2015**, *15* (11), 7567–7573.

(54) Branny, A.; Kumar, S.; Proux, R.; Gerardot, B. D. **2016**, No. May, 1–7.

(55) Palacios-Berraquero, C.; Kara, D. M.; Montblanch, A. R.-P.; Barbone, M.; Latawiec, P.; Yoon, D.; Ott, A. K.; Loncar, M.; Ferrari, A. C.; Atature, M. **2016**, No. May, 1–6.

ToC Figure